ELSEVIER

Journal of Nuclear Materials 247 (1997) 50–58

journal of nuclear materials

Migration behavior of palladium in uranium dioxide

Mitsuru Yoneyama [a], Seichi Sato [a,*], Hiroshi Ohashi [a], Toru Ogawa [b], Akinori Ito [b], Kousaku Fukuda [b]

[a] *Division of Quantum Energy Engineering, Graduate School of Engineering, Hokkaido University, Sapporo 060, Japan*
[b] *Department of Chemistry and Fuel Research, Tokai Research Establishment, Japan Atomic Energy Research Institute, Tokai-mura, Naka-gun, Ibaraki-ken 319-11, Japan*

Abstract

The migration behavior of palladium in UO_2 was investigated by determining the concentration profiles of Pd in UO_2 at temperatures from 1573 to 2073 K in Ar + 3% H_2. Pd was found exclusively in the pores of UO_2. The maximum penetration depth of Pd was more than 100 μm for the pellet of 90% TD and about 50 μm for the pellet of 95% TD for 100 h at 1623 K. Melted Pd wetted UO_2 well and U was detected both in precipitates and in Pd sources, forming an α-Pd phase containing U at about 10 at.%. On the basis of thermodynamic calculations, it was found that a UPd_3 and Pd alloy containing U can form even under the oxygen potential, where O/U ratios were slightly higher than 2.00, say 2.000–2.003. From the above results, a model of the gaseous diffusion of Pd through pores in UO_2 retarded by the formation of U–Pd alloy was proposed. © 1997 Elsevier Science B.V.

1. Introduction

Coated fuel particles, which are utilized for the nuclear fuels of the HTGR, contain four layered coats including a silicon carbide (SiC) layer around fuel kernels. The SiC layer plays an important role in retention of fission products. In the fuels with lower enrichment, the proportion of fission of ^{239}Pu is larger than in the fuels with higher enrichment and the yield of noble metal fission products is larger.

Consequently, since the 1970s the corrosion of the SiC layer with one of the noble metal fission products, palladium (Pd), has come to be paid attention to [1–7]. It has been found that palladium easily penetrates pyrolytic carbon (PyC) layers without any retention and corrodes the SiC layer [2] to decrease the ability of the confinement of fission products. Pearson et al. have reported that the corrosion of the SiC layer with palladium depends only on temperature and does not depend on the difference in the morphology of fuel kernels [3].

From the results of the subsequent out-of-reactor experiments and the thermodynamic considerations [4], it was inferred that the reaction was expressed as $2Pd + SiC \rightarrow Pd_2Si + C$ and it was suggested that the rate of the reaction was controlled by the rate of release of Pd from UO_2 kernels [2,4]. Palladium exists mainly as the Mo–Ru–Rh–Tc–Pd alloy in the kernels [1]. However, palladium is relatively susceptible to release from fuel kernels. This may be due to high vapor pressure of Pd in the alloy [3].

Although these investigations indicate the reaction between Pd and SiC, the rate and mechanism of the migration of Pd in UO_2 have not yet been clarified. Therefore, we have investigated the migration behavior of Pd in UO_2, determined the diffusion coefficient of palladium in UO_2 and proposed a model on migration of Pd in UO_2 on the basis of microstructural observation and thermodynamic consideration, as well as the experiments on migration of Pd.

2. Experimental

2.1. Samples

Two kinds of UO_2 pellets were used as samples. Sample A is the UO_2 pellet of 90.6% TD and sample B is the UO_2 pellet of 95.4% TD. The density, crystal grain

* Corresponding author. Fax: +81-11 706 7139; e-mail: sato@hune.hokudai.ac.jp.

0022-3115/97/$17.00
PII S0022-3115(97)00093-7

Table 1
Samples and heat treatment conditions

Sample batch no.	Sub-sample no.	Heat treatment condition			Experimental	Remarks on sample
		temp. (K)	time (h)	atmosphere		
1 (A pellet)	1-1	1573	60, 100	Ar + 3% H_2	diffusion couples for Pd migration in UO_2	density (g/cm^3), 9.94 ± 0.01 (90.6%TD)
	1-2	1623	100			Grain size (μm), 1–10, 3.3 (mean)
	1-3	1673	20, 60, 100			O/U ratio, 2.00
	1-4	1723	200			Specific area (cm^2/g), 280
	1-5	2073	7.5	vacuum	Pd–UO_2 reaction	Open pore length (μm) [a], 330
2 (B pellet)	2-1	1573	60, 100	Ar + 3% H_2	diffusion couples for Pd migration in UO_2	density (g/cm^3), 10.45 ± 0.01 (95.4% TD)
	2-2	1623	100			Grain size (μm), 2–25, 14.6 (mean)
	2-3	1673	20, 60, 100			O/U ratio, 2.00
	2-4	1723	200			Specific area (cm^2/g), 20
						Open pore length (μm) [a], 50
3	3-1	1953	–	vacuum	Pd melting on UO_2	34.7 mg Pd on UO_2 (A pellet)
4	4-1	1673	19	Ar + 3% H_2	Pd–UO_2 reaction	mixed Pd–UO_2 (Pd:U = 3:1)
	4-2	1673	6	air + 3%H_2		fabricated by inner-gelation process, 1 at.% Pd

[a] Measured by resin penetration method.

size, O/U ratio, specific surface area and the length of open pores of the UO_2 pellets were measured.

The density was measured by immersion gravimetry. The crystal grain size was measured using the method by Underwood [8] and the crystal grain size d_L was calculated by the equation $d_L = 1.78 \times L_T/(P \times M)$ where L_T is the circumference of the circle, P is the number of crystal grains intersecting the circle and M is the magnification of the optical micrograph [9]. The O/U ratio was determined by measuring the weight gain during oxidation [10] and using the method proposed by McNeilly and Chikalla [11]. The specific surface area was measured by BET method. The length of the open pores was represented by the depth of intrusion of a resin.

The characteristics of the UO_2 samples, determined by the above mentioned methods, are shown in Table 1. The concentration of impurities in UO_2 samples are shown in Table 2. The nominal purity of palladium was 99.95%.

2.2. Experimental procedures

Three kinds of experiments were carried out, including the migration of palladium in UO_2, melting of palladium on UO_2 and observation of the formation of the U–Pd alloy. The samples used in these experiments are shown in Table 1, together with the heat treatment (diffusion annealing) conditions.

The surfaces of samples were observed by SEM and

Table 2
Chemical analysis of impurities in A and B pellets

A pellet (sample 1)		B pellet (sample 2)					
element	measured value	element	measured value	element	measured value	element	measured value
Al	16	Ag	< 0.5	F	< 1	Dy	< 0.05
Ca	35	Al	< 10	Fe	< 20	Eu	< 0.05
Co	4	B	< 0.4	Mg	< 4	Gd	< 0.05
Cr	< 1	C	< 10	Mo	< 5	Sm	< 0.05
Cu	< 1	Ca	< 6	N	< 10	H	0.18
Fe	< 1	Cd	< 0.1	Ni	< 12	E.B.C	< 0.7
Mg	< 1	Cl	< 10	Pb	< 6	volatile	< 3
Mo	5	Cr	< 5	Si	< 6	elements	
Si	63	Cu	< 4	Sn	< 3		

EPMA and X-ray diffraction, to detect whether any alloy and intermetallic compounds were formed or not. In X-ray diffraction, a Cu target was used; the voltage and the current were 40 kV and 100 mA, respectively.

2.2.1. Migration of Pd in UO_2

A UO_2 pellet was cut into wafers and the surface of the wafers were abraded with emery paper, No. 600, No. 800 and No. 1000, and with diamond paste, 2.5 and 1.0 μm, successively.

To prepare the diffusion couples with tight contact, palladium vapor was first deposited on the abraded UO_2 surface to a thickness of about 100 nm, after the peripheral sides of the UO_2 wafers were wrapped with aluminum foil. A palladium foil of 50 μm in thickness was annealed at 773 K for 30 min to ensure tight contact with UO_2 wafer. Then the palladium foil was sandwiched between the UO_2 wafers. A diffusion couple was fixed in a Mo jig and placed in an alumina crucible in an alumina tube.

The diffusion couples were kept at temperatures between 1573 and 1723 K for 20 to 200 h under an atmosphere of Ar + 3% H_2 flowing at 1×10^{-4} m^3/min. One different heating was carried out at 2073 K for 7.5 h, in a high frequency induction furnace in a vacuum (0.53–9.3 Pa).

The temperature of the diffusion couples was measured with a Pt–Pt/10% Rh thermocouple covered with an alumina protection tube and controlled within ±5 K.

After heating, the diffusion couples were embedded in resin and cut perpendicular to the Pd/UO_2 interface after the resin was solidified. The surface of the cross-section was abraded in a similar manner to the UO_2 wafers. The concentration profile of Pd was determined by EPMA and the microstructure of the UO_2 surface was observed with an optical microscope and SEM.

In the EPMA observations, line analyses were carried out horizontally to the UO_2 surface over a range of more than 420 μm and up to the depth, where Pd was detectable, at about 3 μm interval. The area of the peak was determined by approximating to either a triangle or a trapezoid. The area of the peaks does not indicate the absolute concentration of Pd, but it is assumed that the area is proportional to the concentration of Pd. In the expression of the concentration of Pd, the sum of the areas of peaks was normalized to the area of 50×300 μm.

2.2.2. Melting of Pd on the surface of UO_2

In order to determine the extent to which Pd may wet UO_2, a piece of Pd of 34.7 mg was put on the surface of a UO_2 wafer, heated at a rate of 60 K/min in the induction furnace. The piece of Pd has been melted and a Pd droplet formed, then it was cooled immediately after attainment to 1953 K. The UO_2 wafer with the solidified Pd on it was cut in the middle and the morphology was observed.

2.2.3. Observation of formation of U–Pd alloy

Microstructual observations of the diffusion couples after annealing were carried out by EPMA to examine whether any U–Pd alloy has been formed or not. In addition, Green pellets formed from Pd and UO_2 mixed powder were heated as shown for sample No. 4 in Table 1, and were examined by EPMA and X-ray diffraction.

3. Results

3.1. Migration of Pd in UO_2

The microstructures near the Pd/UO_2 interface are shown in Fig. 1. It was observed that Pd was deposited in the pores in UO_2 and wetted UO_2 walls well. Although some parts of the Pd source have disappeared in some diffusion couples, the Pd source has almost remained after heating.

The results of the line analysis and SEM observations of the vicinity of the Pd/UO_2 interface were shown in Fig. 2. It is clear that palladium distributes exclusively near the interface and it seems that the concentration of Pd decreases with the distance from the Pd/UO_2 interface, as can be seen from the concentration profiles of Pd shown in

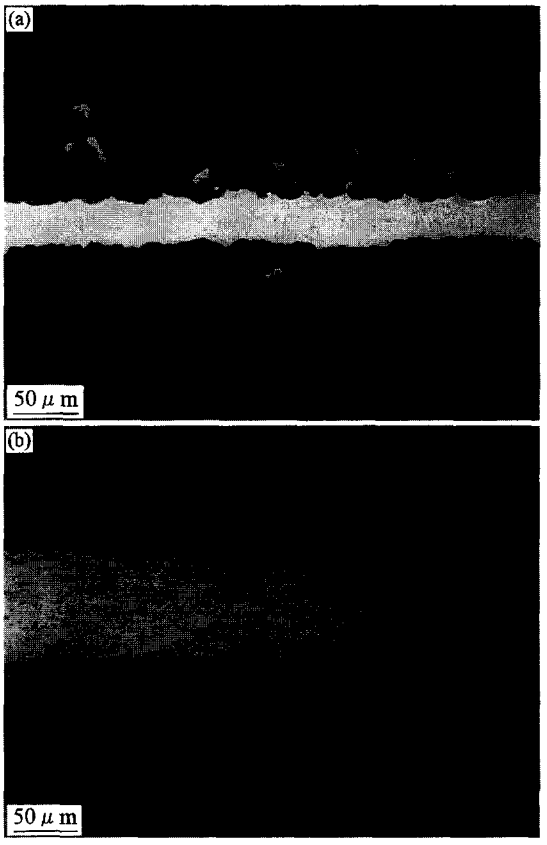

Fig. 1. Optical micrograph of Pd/UO_2 wafer interface.

Fig. 3. The profile rather well reproduces the results of the line analyses. In the pellets of 95% TD, Pd did not penetrate very deeply. The depth of penetration with a relatively large amount of Pd was more than 100 μm for the pellets of 90% TD and about 50 μm for the pellets of 95% TD.

3.2. Melting of Pd on the surface of UO_2

The optical micrograph of the cross-section of Pd melted on the surface of UO_2 is shown in Fig. 4. Pd wetted the surface of UO_2 very well. Especially at the tip of Pd, Pd deeply penetrated into UO_2.

3.3. Formation of U–Pd alloy

3.3.1. Observation by SEM and EPMA

Fig. 5 shows the typical SEM images near the Pd sources of samples 1–4 and the results of line analysis by EPMA. Uranium was detected in all regions of the metallic precipitates in UO_2 and the Pd sources, everywhere Pd exists.

In Fig. 5, the Pd source is able to be divided roughly into two parts by the contrast in SEM images. The EPMA intensities for U and Pd were measured both in light and

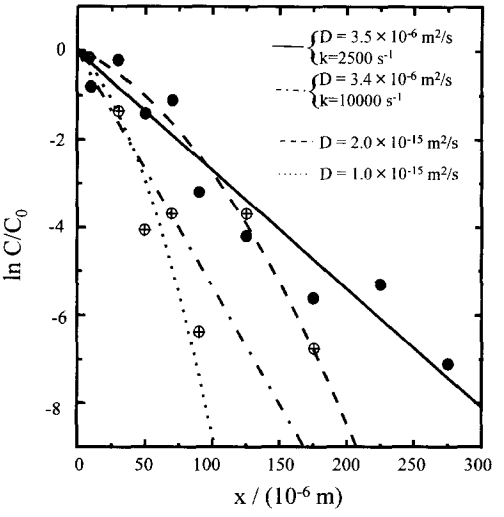

Fig. 3. Concentration profile of Pd in UO_2 as a function of penetration depth from UO_2 /Pd interface; (⊕) 90% TD at 1623 K for 100 h; (●) 90% TD at 1723 K for 200 h; (---) and (— — —) are obtained from simple diffusion model; (————) and (– · –) are obtained from the present model based on gas phase diffusion of Pd in UO_2 and Pd trapping by formation of U–Pd alloy.

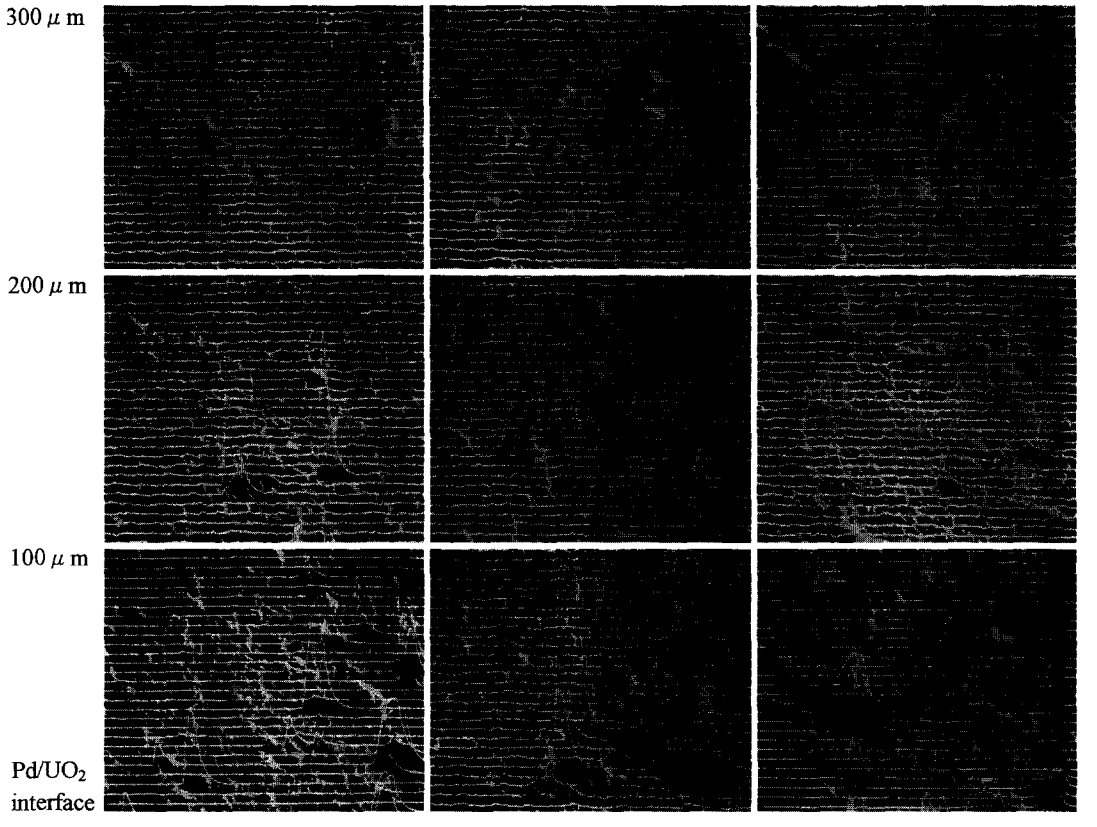

Fig. 2. Typical example of line analysis of Pd with electron probe microanalyzer on scanning electron micrograph of UO_2 in contact with Pd source (90% TD, 100 h, 1623 K).

dark parts and ZAF correction was made; the concentration of U was 10.4 at.% in the light part and 0.8 at.% in the dark part.

The precipitates formed in UO_2 were also able to be divided into two parts, light and dark, in a similar manner. In larger precipitates, the diameters of which are as large as 20 μm, two phases frequently coexisted (Fig. 5c).

In samples 1-1 and 1-3, almost all regions of the Pd source showed the composition of the light part, dark part of several μm and eutectic-like microstructure (sample 1-1) and pores in the Pd source were observed. The concentration of U in the eutectic-like microstructures differed from phase to phase, but the difference was within about 10%. In sample 3-1, a homogeneous phase containing U at 6.8% was observed.

3.3.2. Identification of alloy by X-ray diffraction

The peaks of Pd are somewhat broad in sample 1-1. Further, the positions of the peaks shift from the inherent positions for Pd; the lattice parameter calculated for Pd from the positions of the observed peaks was 0.393–0.396 nm, although the lattice parameter reported for pure Pd is 0.389 nm [12]. The peaks for the stoichiometric metallic compound such as UPd_3 [13,14] were not identified. Further, the evidence that a part of the sample melted and a liquid phase formed, was observed for sample 4-1.

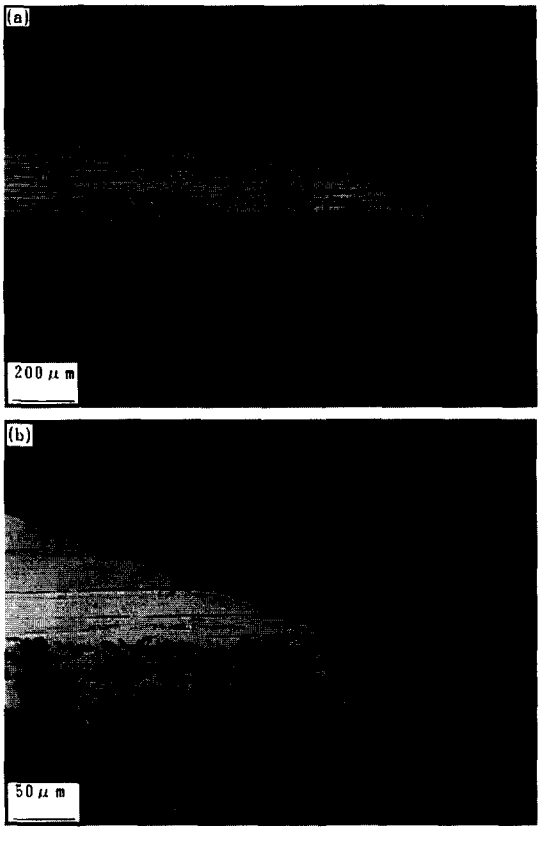

Fig. 4. Cross-sectional optical micrograph of Pd, after melting on UO_2 at 1953 K and solidification under vacuum.

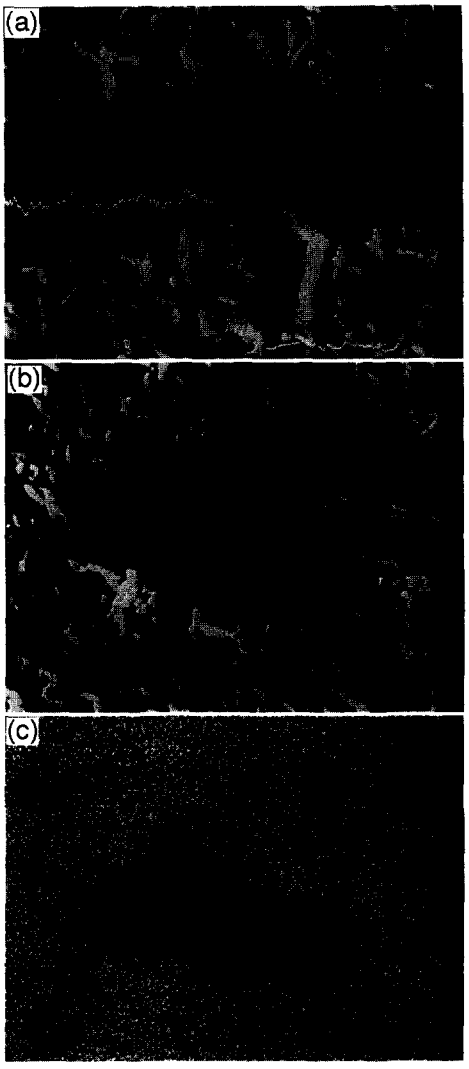

Fig. 5. SEM/EPMA micrograph of Pd in contact with UO_2 (sample 1–4 in Table 1) (a) SEM and EPMA-line analysis in Pd source; (b) SEM precipitate of Pd in a pore in UO_2; (c) characteristic X-ray pattern of uranium (U-M_β) in the microstructure (b).

4. Discussion

4.1. Mechanism of transport of Pd in UO_2

4.1.1. Analysis by simple diffusion

It was found that the density of UO_2 pellets strongly affects the migration of Pd in UO_2. The depth of penetration of Pd was comparable to the open pore length mea-

sured by resin penetration, 50 μm, in the UO_2 pellet of 95% TD. In the UO_2 pellet of 90% TD, the depth of penetration of Pd, more than 100 μm, was shorter than that of resin, 330 μm (Table 1).

Many metallic precipitates of 10–20 μm in diameter were observed in the pores in UO_2, as can be seen from Fig. 1(a) and (b). It is very likely that almost all Pd penetrates UO_2 via pores. Further, it is also considered that Pd migrates in the gas phase, since the vapor pressure of Pd is relatively high as 4.76×10^{-1} Pa at 1673 K [15].

First, the constant-source diffusion model was applied to the concentration profiles of Pd in UO_2, since the source of Pd remained sufficiently after the diffusion annealing. In this case, the Fick's second law

$$\partial C/\partial t = D\partial^2 C/\partial X^2 \quad (1)$$

is applicable with the conditions, $C(x, 0) = 0$, at $x > 0$ and $C(0, t) = C_0$, $t > 0$. Here, C is the concentration of Pd at the distance from Pd/UO_2 interface, x, D is the apparent diffusion coefficient of Pd in UO_2 and t is the annealing period.

The solution of Eq. (1) is

$$C = C_0 \operatorname{erfc}\{x/2\sqrt{Dt}\}, \quad (2)$$

where C_0 is the concentration of Pd at the Pd/UO_2 interface.

The result of the analysis for a typical experimental result is shown in Fig. 3. In the pellets of 90% TD, the simple diffusion model is not applicable, because Eq. (2) can not represent all experimental data. In addition, the values of the diffusion coefficient obtained with Eq. (2) are between 10^{-16}–10^{-13} m^2/s at temperatures between 1573–2073 K.

Instead, the theoretical estimation of the diffusion coefficient of palladium, D^*, was carried out with a hypothesis of the diffusion in gas phase by the equation

$$D^* = \lambda^2 \Gamma/6, \quad (3)$$

where λ is the mean free path of Pd in gas phase and Γ the collision frequency. Here λ is obtained from

$$\lambda = 1/\left\{\pi \sum \sigma(i)^2 n(i)\right\}, \quad (4)$$

where $\pi\sigma(i)^2$ is the collision cross-section of an i molecule in the gas phase and $n(i)$ is the number of molecules in the unit volume. Further, the collision frequency Γ is expressed as

$$\Gamma = \bar{v}/\lambda = (1/\lambda)\sqrt{(8RT/\pi M)}, \quad (5)$$

where v is the average velocity of atomic Pd, M the atomic weight of Pd, R the gas constant and T the absolute temperature.

Since the atmosphere of the system is a mixture of 97% Ar and 3% H_2 at 0.1 MPa, the partial pressure of Pd is 4.76×10^{-1} Pa at 1673 K, λ is 3.55×10^{-2} μm and Γ is 1.62×10^{10} s^{-1}. Therefore, for the diffusion of Pd in gas phase, the diffusion constant D^* is obtained as

$$D^* = \lambda^2 \Gamma/6 = 3.4 \times 10^{-6} \text{ m}^2/\text{s}. \quad (6)$$

This theoretical result is very large compared to the experimental results. This means that there may be some retarding factors, against gaseous diffusion of Pd. The following are considered as retarding factors: (1) the geometry of pores in UO_2 such as the limited length of open pores which restricts the migration of Pd in UO_2, (2) the trapping effect on Pd migration due to the penetration of gaseous Pd into very small connected or dead-end pores and (3) possible trapping of Pd on the inner surface of UO_2 pores by forming a U–Pd alloy as a result of the reduction of UO_2.

Since, in the UO_2 pellet of 95% TD, the depth of Pd penetration is considerably small compared to that in the pellet of 90% TD and in addition the depth of penetration of Pd is comparable to the depth of that of resin, the geometry of pores may strongly affect the migration of Pd. However, it is considered that the effect of the geometry is small for the UO_2 pellet of 90% TD, since the depth of penetration of Pd is smaller than that of the resin. If factor (2) is responsible, it is likely that palladium uniformly distributes on the wall of UO_2 and in this case the local precipitation of Pd, such as shown in Fig. 1, cannot be interpreted. Factor (3) is considered to be the case, where Pd vapor is trapped and forms a Pd-containing alloy. Only U–Pd and Si–Pd alloys are considered, since no detectable element was observed except for Si (0.036 wt%) when measuring for impurities.

4.1.2. Formation of U–Pd alloy

From the reason described in Section 4.1.1, the experiment in Section 2.2.3 was performed to examine whether a U–Pd alloy is formed or not. Further, apart from this experiment, we examined the condition of formation of a U–Pd alloy from the thermodynamic point of view, which will be described later.

It was found that the concentration of U in Pd in diffusion couples is 1–10 at.% after diffusion annealing and it was considered that U dissolves in Pd to form α-Pd solid solution, from the phase diagram of the U–Pd system [16,17].

In the samples 1-1 and 1-3, the concentration of U was about 10 at.% in almost all regions. The peak of α-Pd was also found in these samples by X-ray diffraction. The lattice parameters calculated from the peak positions, 0.393–0.396 nm, were in agreement with the results by Catterall who investigated the relationship between the lattice parameter of α-Pd and U concentrations [18]. Further, the width of the peak at half height was somewhat large, suggesting some scatter in the composition of the U–Pd alloy.

It is considered that the temperature in the experiment

might be in the coexistence region of the liquid and solid α-Pd phases, due to freezing point depression by dissolution of U from UO_2 to Pd, although the melting point of the pure Pd is 1828 K. It may be the reason that Pd wetted UO_2 well in Figs. 1 and 4.

On the other hand, the eutectic-like microstructures were partly observed in the sample heated at 1573 K (sample 1-1). From the phase diagram it is understandable that the eutectic α- and ε-phases appeared at 1573 K. It is more reasonable to consider that the χ-phase appeared during cooling because the concentration of U is about 10 at.% and the difference in the concentration of U is small among the phases. In other locations, round dips were observed, which may be the evidence that gas existed. It is quite possible that the dips are the pores filled with H_2O, the by-product of the reaction between UO_2 and Pd under the reducing atmosphere.

In sample 3-1, a homogeneous α-Pd phase containing U at 6.8 at.% was observed. The reason that the concentration of U is less than that in the other samples may be due to the slightly oxidizing atmosphere.

In the sample heated at 1723 K, a two-phase alloy was observed and Si was detected at about 20 at.% in one phase. Si was originally contained in Pd foil as an impurity and the concentration of Si in Pd was 0.036 wt% (1.08 at.%) on average. The phase containing more Si than 10 at.% occupied a rather large region, possibly resulted from the Pd source containing a large mass of Si. The phase was not observed in the other samples. Judging from the phase diagram, UPd_3 is a stable U–Pd alloy at high temperatures and has actually been observed in UC_2 fuels [3]. In our experiments, although the formation of UPd_3 was not observed, it is considered that the above mentioned alloy formed because of the high stability of UPd_3, $\Delta G_f(UPd_3) = -321$ kJ/mol at 1323 K [17] and -520 kJ/mol at 1600 K [19].

4.1.3. Analysis by alloy formation model

The trapping of Pd vapor by alloy formation is assumed to play an essential role on the remarkable retardation of vapor phase transport of Pd, therefore the Fick's second law is modified to analyze the experimental results:

$$\partial C/\partial t = D\partial^2/\partial x^2 - kC, \tag{7}$$

where k is the trapping rate constant. The initial and boundary conditions are $C(x, 0) = 0$ at $x > 0$; $C(0, t) = C_0$ for $t > 0$. Then, the solution of Eq. (7) is [20,21]

$$C = (C_0/2)\left\{\exp\left(-x\sqrt{k/D}\right)\mathrm{erfc}\left(x/2\sqrt{Dt} - \sqrt{kt}\right) + \exp\left(x\sqrt{k/D}\right)\mathrm{erfc}\left(x/2\sqrt{Dt} + \sqrt{kt}\right)\right\}. \tag{8}$$

An example of the results obtained by using this equation is shown in Fig. 3. In this procedure, the diffusion coefficient D theoretically obtained from Eq. (3) was used and the rate constant k was determined by a least squares method, using Eq. (8). The obtained k values are shown in Table 3.

Table 3
Pd trapping rate constant, k

Temperature (K)	k (s^{-1})
2073	9.5×10^{3}
1723	2.5×10^{3}
1673	1.7×10^{4}
1623	1.0×10^{4}
1573	1.2×10^{4}

The obtained k values do not show regularity with respect to temperature. Therefore, further discussion is not possible for the formation of a U–Pd alloy. However it is important that the model calculation performed by introduction of the rate constant k for the trapping of Pd can reproduce the experimental concentration profiles up to furthest distances from the Pd/UO_2 interface.

4.2. The thermodynamics of formation of U–Pd alloy

In a similar investigation, Yang and Olander [22] examined the transport of Ru in UO_2 and they reported that the alloy URu_3 formed in UO_2. Further, they evaluated the condition for the formation of URu_3 thermodynamically and they found that the O/U ratio is less than 1.999 at 2020 K for the condition of the formation of URu_3.

It can be seen that from the comparison of the Gibbs free energies of formation of U alloys, the thermodynamic stability is in the order of U–Pd, U–Rh and U–Ru systems [19,23]. Therefore, we examined the condition under which UPd_3 can be formed. The procedure is shown as follows.

The equations expressing the formation of UPd_3 are

$$UO_2 + \frac{x}{2}O_2 \rightarrow UO_{2+x} \tag{9}$$

and

$$UO_{2+x} + 3Pd \rightarrow UPd_3 + \frac{2+x}{2}O_2. \tag{10}$$

From Eqs. (9) and (10),

$$UO_2 + 3Pd \rightarrow UPd_3 + O_2 \tag{11}$$

is obtained. On the other hand, the equation

$$UO_{2+x} + \frac{dx}{2}O_2 \rightarrow UO_{2+x+dx} \tag{12}$$

applies. When the equilibrium is attained in Eq. (12), the balance of the chemical potential is

$$\mu(UO_{2+x}) + \frac{dx}{2}\mu(O_2) = \mu(UO_{2+x+dx}). \tag{13}$$

Here,

$$d\mu(UO_{2+x}) = \frac{1}{2}\mu(O_2)\,dx, \tag{14}$$

$$\int_0^x d\mu(UO_{2+x}) = \frac{1}{2}\int_0^x \mu(O_2)\,dx. \tag{15}$$

Therefore,

$$\mu(UO_{2+x}) - \mu(UO_2) = \frac{1}{2}\int_0^x \mu(O_2)\,dx. \tag{16}$$

When the equilibrium is attained in Eq. (10),

$$\mu(UO_{2+x}) + 3\mu(Pd) = \mu(UPd_3) + \frac{2+x}{2}\mu(O_2) \tag{17}$$

applies. From Eqs. (16) and (17),

$$\mu(UPd_3) = \mu(UO_2) + \frac{1}{2}\int_0^x \mu(O_2)\,dx - \frac{2+x}{2}\mu(O_2) + 3\mu(Pd) \tag{18}$$

is obtained. On the other hand,

$$\mu(UPd_3) = \Delta G_f^0(UPd_3) + \mu^0(U) + 3\mu^0(Pd), \tag{19}$$

$$\mu(UO_2) = \Delta G_f^0(UO_2) + \mu^0(U) + \mu^0(O_2), \tag{20}$$

$$\mu(O_2) = \mu^0(O_2) + \Delta\bar{G}(O_2). \tag{21}$$

From these equations,

$$\Delta G_f^0(UPd_3) + \mu^0(U) + 3\mu^0(Pd) = \Delta G_f^0(UO_2) + \mu^0(U) + \mu^0(O_2) + \frac{1}{2}\int_0^x \{\Delta\bar{G}(O_2) + \mu^0(O_2)\}\,dx - \frac{2+x}{x}\Delta\bar{G}(O_2) - \frac{2+x}{2}\mu^0(O_2) + 3\mu(Pd). \tag{22}$$

Here, if $\mu(Pd)$ can be regarded to be $\mu^0(Pd)$.

$$\Delta G_f^0(UPd_3) = \Delta G_f^0(UO_2) + \frac{1}{2}\int_0^x \Delta\bar{G}(O_2)\,dx - \frac{2+x}{2}\Delta\bar{G}(O_2) \tag{23}$$

is obtained.

Calculation was carried out based on Eq. (23) using the Gibbs free energies of formation $\Delta G_f^0(UO_2) = -807$ kJ/mol [19]; $\Delta G_f^0(UPd_3) = -520$ kJ/mol at 1600 K [19] or -321 kJ/mol at 1323 K [17] and the oxygen potential of UO_{2+x} [24,25]. The UPd_3 alloy can be formed thermodynamically at 1673 K even under the condition where the oxygen potential is slightly higher than that for stoichiometric UO_2, i.e., $UO_{2.003}$, using the former $\Delta G_f^0(UPd_3)$, while $UO_{2.000}$ in the latter. In the present experimental condition, instead of UPd_3, an α-Pd(U) alloy whose uranium activity is lower than that in UPd_3 is formed. Therefore, it is quite possible that slightly hyper-stoichiometric UO_2 is reduced in contact with the Pd metal to form α-Pd(U) alloy which works as a trap of Pd in vapor phase transport in UO_2.

5. Conclusions

The migration behavior of palladium in UO_2 was investigated by determining the concentration profiles of Pd in UO_2 at temperatures from 1573 to 2073 K in Ar + 3% H_2. Pd was found exclusively in the pores of UO_2.

For the UO_2 pellets of 90% TD, the length of open pores is larger than the penetration depth of Pd. Melted Pd wetted UO_2 well and U was detected by microstructual observation both in precipitates and in Pd sources, forming an α-Pd phase containing U at about 10 at.%. Furthermore, the apparent diffusion coefficient of Pd was much smaller than the evaluated values via vapor phase diffusion.

On the other hand, for the UO_2 pellets of 95% TD, Pd penetrates up to only 50 μm at our experimental conditions because of the geometrical restriction of the length of open pores.

A model consisting of vapor phase diffusion of Pd through pores in UO_2 and trapping process by formation of U–Pd alloy during the diffusion was proposed to elucidate the measured concentration profiles of Pd in the UO_2 pellets of 90% TD. It was clarified that the model calculation well reproduced the experimental concentration profiles of Pd in UO_2.

On the basis of thermodynamic calculations using available data, UPd_3 is found to be formed, even under the oxygen potential, where O/U ratios are slightly higher than 2.00, say 2.000–2.003.

References

[1] J.I. Bramman et al., J. Nucl. Mater. 25 (1968) 201.
[2] K. Minato et al., J. Nucl. Mater. 172 (1990) 184.
[3] R.L. Pearson et al., ORNL/TM-6991, 1980.
[4] T. Ogawa, JAERI-M 82-098, 1982.
[5] M. Takada et al., JAERI-M 90-113, 1990.
[6] T.N. Tiegs, Nucl. Technol. 57 (1982) 389.
[7] K. Minato et al., JAERI-M 84-002, 1984.
[8] E.E. Underwood, in: Metals Handbook, 9th Ed., Vol. 9, ed. K. Mills et al. (American Society for Metals, Metals Park, OH, 1985) p. 123.
[9] W. Rostoker, J.R. Dvorac, Interpretation of Metallographic Structures (Academic Press, New York, 1977).
[10] JAERI, JAERI 4053, 1971.
[11] C.E. McNeilly, T.D. Chikalla, J. Nucl. Mater. 39 (1971) 77.
[12] H.E. Swanson et al., NBS Circ. 539 (1953) 95.
[13] P. Villars, L.D. Calvert, Person's Handbook of Crystallographic Data for Intermetallic Phases, 2nd Ed. (American Society for Metals, Metals Park, OH, 1985).
[14] T.J. Heal, G.I. Williams, Acta Crystallogr. 8 (1955) 494.

[15] O. Kubaschewski, C.B. Alcock, Metallurgical Thermochemistry, 5th Ed. (Pergamon, New York, 1979).
[16] T.B. Massalski, ed., Binary Alloy Phase Diagrams, 2nd Ed. (The Materials Information Society, 1990).
[17] H. Kleykamp, S.G. Kang, J. Nucl. Mater. 230 (1996) 280.
[18] J.A. Catterall, Philos. Mag. 2 (1957) 491.
[19] E.H.P. Cordfunke, R.J.M. Konings, Thermochemical Data for Reactor Materials and Fission Products (North-Holland, Amsterdam, 1990).
[20] J. Crank, The Mathematics of Diffusion, 2nd Ed. (Clarendor Oxford, 1975).
[21] R.S. Rodliffe, Rd/B/N2375, 1972.
[22] R.L. Yang, D.R. Olander, Nucl. Technol. 54 (1981) 223.
[23] H. Kleykamp, J. Nucl. Mater. 201 (1993) 193.
[24] K. Park, D.R. Olander, High Temp. Sci. 29 (1990) 203.
[25] P.E. Blackburn, J. Nucl. Mater. 46 (1973) 244.